Contribution from the Department of Chemistry,
Indian Institute of Technology, Madras 600 036, India

# Crystal and Molecular Structure of Dimeric Bis[*N*,*N*-di-*n*-propyldithiocarbamato]zinc(II) and the Study of Exchange-Coupled Copper(II)–Copper(II) Pairs in Its Lattice

N. Sreehari, Babu Varghese, and P. T. Manoharan*

*Received October 5, 1989*

The crystal and molecular structure of dimeric bis[*N*,*N*-di-*n*-propyldithiocarbamato]zinc(II) at room temperature has been determined. There are two molecular dimeric units in a monoclinic cell, $a$ = 12.156 (7) Å, $b$ = 14.488 (9) Å, $c$ = 12.506 (8) Å, $\beta$ = 111.50 (3)°, with space group $P2_1$. In the dimeric unit the zinc atoms share sulfur atoms and each zinc atom is coordinated with five sulfur atoms in a distorted trigonal-bipyramidal environment. The two zinc atoms in the dimeric unit are separated by a distance of 3.786 Å. The triplet-state EPR studies of copper(II)–copper(II) pairs in this lattice indicate that the nature of isotropic exchange coupling is ferromagnetic with a magnitude of +13 $cm^{-1}$ and that the host lattice undergoes contraction at lower temperatures. The exact magnitude of exchange coupling was derived by an analysis of the EPR signal intensities of half-field transitions ($\Delta M_s = \pm 2$).

## Introduction

There has been a growing interest in recent years to study magneto-structural correlations in a series of exchange-coupled transition metal ion dimeric systems. It has been established by a host of workers[1-4] by studies on a variety of binuclear (or dimeric) complexes that even a small structural change in these dimers (even those induced by a change in counterion) can lead to significant changes in the magnitudes of exchange-coupling constants. A number of successful attempts have been made in the past to understand the mechanism of magnetic exchange interactions in different series of copper(II) dimeric systems with a variety of bridging groups like hydroxyl, oxalato, azido, fluoro, chloro, sulfido, etc.[5]

Among the sulfido-bridged copper(II) dimeric systems bis[*N*,*N*-diethyldithiocarbamato]copper(II), $[Cu(dedtc)_2]_2$, is the most widely studied system. There are many reports on the EPR studies of isolated $Cu^{2+}$–$Cu^{2+}$ pairs in dimeric bis[*N*,*N*-diethyldithiocarbamato]zinc(II), $[Zn(dedtc)_2]_2$.[6-13] These studies have shown the presence of spin–spin interactions between the two metal centers of the dimeric unit. Triplet-state EPR spectra arising from spin–spin interactions have been measured on many systems. Recently, we have reported the triplet-state EPR studies of $Cu^{2+}$–$Cu^{2+}$ pairs in the lattice of dimeric bis[*N*,*N*-diisopropyldithiocarbamato]zinc(II), $[Zn(dipdtc)_2]_2$.[14] In continuation of our work, we are now reporting the crystal and molecular structure of another related dimeric system, bis[*N*,*N*-di-*n*-propyldithiocarbamato]zinc(II), $[Zn(dnpdtc)_2]_2$, and also the EPR studies of $Cu^{2+}$–$Cu^{2+}$ pairs in this lattice.

The crystal and molecular structures of a number of bis[*N*,*N*-dialkyldithiocarbamato]copper(II) and -zinc(II) complexes have been reported. The copper(II) and zinc(II) dimethyldithiocarbamato complexes were found to have polymeric structures.[15,16] The diethyldithiocarbamato complexes of copper(II) and zinc(II) are dimeric in nature with slight differences in bonding pattern.[17,18] Bis[*N*,*N*-di-*n*-propyldithiocarbamato]copper(II) was reported to have dimeric structure.[19] The system bis[*N*,*N*-diisopropyldithiocarbamato]zinc(II) is also dimeric in nature[20] whereas its copper(II) analogue is monomeric in nature.[21] Since there are substantial differences in the nature of bonding pattern among these dialkyldithiocarbamato dimeric systems, they exhibit differing magnetic properties. We have found from the literature that there is no structural report on bis[*N*,*N*-di-*n*-propyldithiocarbamato]zinc(II). Our EPR studies of $Cu^{2+}$ doped in this lattice have given proof for the existence of dimeric units in the host lattice. The complete crystal structure is, therefore, required to understand the EPR tensorial properties of $Cu^{2+}$–$Cu^{2+}$ pairs in this lattice.

**Table I.** Crystallographic Data

| | |
|---|---|
| chem formula: $[Zn(S_2CN(n\text{-}C_3H_7)_2)_2]_2$ | $T$ = 23 °C |
| $(Zn_2S_8N_4C_{28}H_{56})$ | $\lambda$ = 1.5418 Å |
| $a$ = 12.156 (7) Å | $\rho_{obsd}$ = 1.402 g $cm^{-3}$ |
| $b$ = 14.488 (9) Å | $\rho_{calcd}$ = 1.354 g $cm^{-3}$ |
| $c$ = 12.506 (8) Å | $\mu$ = 51.99 $cm^{-1}$ |
| $\beta$ = 111.50 (3)° | |
| $V$ = 2049.28 Å$^3$ | |
| $Z$ = 2 | |

transm factors: max = 0.6157; min = 0.3354 $R(F_o)$ = 0.0477

## Experimental Section

**Preparation of the Compounds.** The bis[*N*,*N*-di-*n*-propyldithiocarbamato]copper(II) and -zinc(II) complexes were prepared by mixing the aqueous solutions of the metal chlorides and sodium salt of the ligands in a 1:2 ratio, as reported in the literature.[22] The precipitate thus formed on mixing the solutions was washed with water, dried, and purified by recrystallization from acetone. The mixed crystals of copper(II) in the zinc(II) lattice in different proportions were grown by the slow evaporation method, using acetone as a solvent.

(1) Crowford, V. H.; Richardson, W. H.; Wasson, J. R.; Hodgson, D. J.; Hatfield, W. E. *Inorg. Chem.* **1976**, *15*, 2107.
(2) Hall, G. R.; Duggan, D. M.; Hendrickson, D. N. *Inorg. Chem.* **1975**, *14*, 1956.
(3) Julve, M.; Verdaguer, M.; Kahn, O.; Gleizes, A.; Philoche-Levisalles, M. *Inorg. Chem.* **1983**, *22*, 368.
(4) Kuppusamy, P.; Manoharan, P. T. *Proc.—Indian Acad. Sci., Chem. Sci.* **1987**, *98*, 115.
(5) See the various articles in: Willett, R. D., Gateschi, D., Kahn, O., Eds. *Magneto-Structural Correlations in Exchange Coupled Systems*; NATO ASI Series; D. Reidel: Dordrecht, The Netherlands, 1985.
(6) Villa, J. F.; Hatfield, W. E. *Inorg. Chim. Acta* **1971**, *5*, 145.
(7) Reddy, T. R.; Srinivasan, R. *J. Chem. Phys.* **1965**, *43*, 1404.
(8) Cowsik, R. K.; Rangarajan, G.; Srinivasan, R. *Chem. Phys. Lett.* **1971**, *8*, 136.
(9) Cowsik, R. K.; Srinivasan, R. *Pramana* **1973**, *1*, 177.
(10) Al'tshuler, S. A.; Kirmse, R.; Solovev, B. V. *J. Phys. C: Solid State Phys.* **1975**, *8*, 1907.
(11) Manjunath, C. V.; Srinivasan, R. *J. Magn. Reson.* **1977**, *28*, 177.
(12) Keijzers, C. P.; van der Meer, P. L. A. Chr. M.; de Boer, E. *Mol. Phys.* **1975**, *29*, 1733.
(13) Keijzers, C. P.; de Boer, E. *Mol. Phys.* **1975**, *29*, 1743.
(14) Sreehari, N.; Manoharan, P. T. *Mol. Phys.* **1988**, *63*, 1077.
(15) Einstein, F. W. B.; Field, J. S. *Acta Crystallogr., Sect. B* **1974**, *B30*, 2928.
(16) Klug, H. P. *Acta Crystallogr.* **1966**, *21*, 536.
(17) Bonamico, M.; Dessy, G.; Mugnoli, A.; Vaciago, A.; Zambonelli, L. *Acta Crystallogr.* **1965**, *19*, 886.
(18) Bonamico, M.; Mazzoni, G.; Vaciago, A.; Zambonelli, L. *Acta Crystallogr.* **1965**, *19*, 898.
(19) Peyronel, G.; Pignedoli, A.; Anolini, L. *Acta Crystallogr., Sect. B* **1972**, *B28*, 3596.
(20) Miyamae, H.; Ito, M.; Iwasaki, H. *Acta Crystallogr., Sect. B* **1979**, *B35*, 1480.
(21) Iwasaki, H.; Kobayashi, K. *Acta Crystallogr., Sect. B* **1980**, *B36*, 1655.
(22) Peterson, R.; Vanngard, T. *Ark. Kemi* **1961**, *17*, 249.

0020-1669/90/1329-4011$02.50/0 

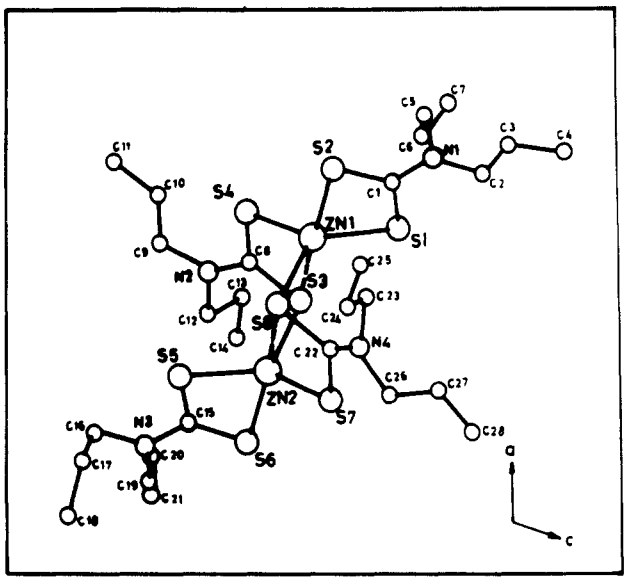


**Figure 1.** Perspective view of the $[Zn(dnpdtc)_2]_2$ molecule down the *b* axis.

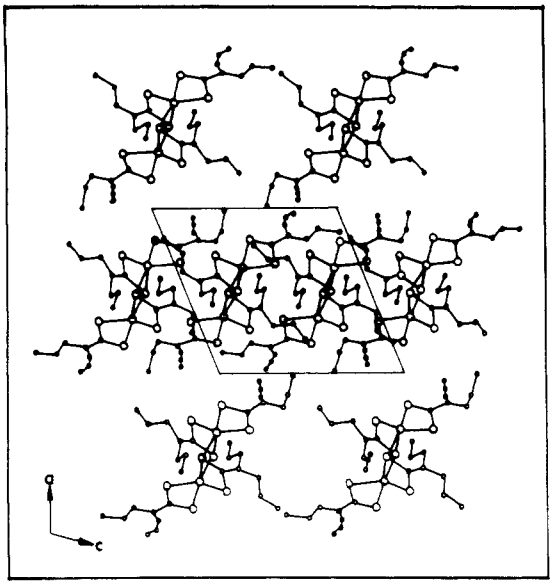


**Figure 2.** Projection of the packing of the molecules viewed down the *b* axis.

**Crystallographic Data Collection and Structure Determination.** The diffraction intensity data were collected by using a computer-controlled Enraf-Nonius CAD-4F, four-circle single-crystal X-ray diffractometer with crystal size of 0.3 × 0.5 × 0.3 $mm^3$ dimensions. The cell dimensions and their standard deviations were obtained by method of shortest vectors, followed by least-squares refinement of 25 high-angle reflections. Intensities were measured at 23 °C by using the $\omega-2\theta$ scan technique with graphite-monochromated Cu K$\alpha$ radiation. The cell is monoclinic. From systematic absences and the test for center of symmetry the space group was confirmed as $P2_1$. The measured density corresponds to two dimeric units per unit cell. Table I shows the crystallographic data of the title compound.

Intensity data were collected for $2° < \theta < 75°$ for a total of 3420 reflections of which 2880 reflections were found to have $I > 3\sigma(I)$. The ranges of *h*,*k*,*l* for which data were collected are $h = -15$ to 15, $k = 0$ to 17, and $l = 0$ to 15.

Numerical absorption correction was applied to the data with the SHELX-76[23] computer program. The structure has been solved by the standard method of heavy atom. As the first step, the Patterson function of the data was obtained as a discrete three-dimensional map and the position of the heavy atom was located. Once the position of the heavy atom was found, the positions of the other atoms, namely sulfurs, nitrogens, and carbons, were located by using Fourier maps and assigning approximate phases to each reflection as the ones calculated from the known part of the structure. This way all the non-hydrogen atoms were located.

Initially the structure was refined (positional coordinates and isotropic thermal parameters) by the principle of least squares with the minimization of the quantity $\sum(|F_o| - k|F_c|)^2$. After every cycle of least-squares refinement, the convergence was tested by the residual parameter defined as

$$R = \frac{\sum||F_o| - k|F_c||}{\sum F_o}$$

When the least-squares refinement with isotropic thermal parameters converged, anisotropic thermal parameters were assigned to each atom and the least-squares procedure was repeated. A difference Fourier map at this stage revealed all hydrogen atom positions. The refinement of the structure with inclusion of positional coordinates and isotropic thermal parameters of hydrogen atoms resulted in a final *R* value of 0.0477. Hughe's weighting scheme was applied for weighted least-squares refinement, but neither the residual factor nor bond parameters were found to improve. Structure solution and refinement were done by using the SHELX-76 computer program. Coefficients of atomic scattering factors for non-hydrogen atoms and anomalous scattering factors are given by Cromer and co-workers,[24,25] respectively. Scattering factor coefficients for hydrogen atoms are taken from the data of Stewart et al.[26]

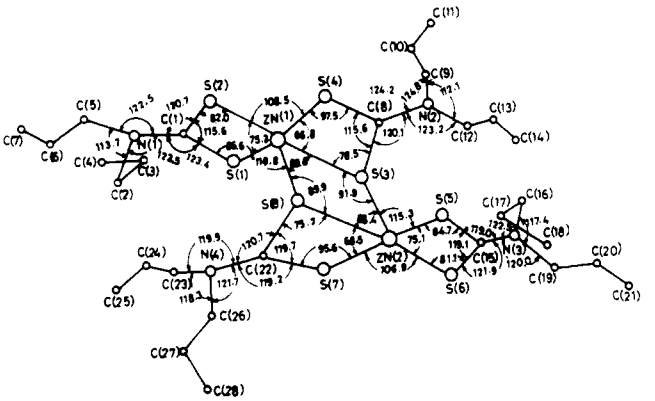


**Figure 3.** Bond lengths (Å) in the $[Zn(dnpdtc)_2]_2$ molecule.

**EPR Measurements.** The EPR measurements were carried out on a Varian E-112 X-band spectrometer working at 8.6–9.5 GHz with 100-kHz field modulation. DPPH ($g = 2.0036$) was used as an internal "*g*" marker. Variable-temperature measurements were performed by using a Varian E-257 variable-temperature accessory and an Oxford low-temperature unit.

For single-crystal work, the crystal was mounted at the end of a quartz rod with Apiezon-N grease or quickfix. It was then introduced into the cavity and rotated on a goniometer device. The axis of rotation was always perpendicular to the magnetic field.

## Results and Discussion

**Description of the Structure.** The final atomic coordinates (fractional) for non-hydrogen atoms are given in Table II. The anisotropic thermal parameters for non-hydrogen atoms are included in the supplementary material. Separate tables of least-square planes and atomic deviations therefrom, some intermolecular contacts, and some relevant torsion angles are given in the supplementary material.

A perspective view of the molecular structure is shown in Figure 1, and the packing of the molecules down the *b* axis (onto the *ac* plane) is shown in Figure 2. The sulfur atoms S(1), S(8), S(2), S(3), and S(4) form an approximate trigonal-bipyramidal environment around Zn(1), with S(1), S(4), and S(8) forming the basal plane and S(2) and S(3) forming the apexes. The metal atom Zn(1) is displaced from the mean S(1), S(4), and S(8) plane through a distance of 0.171 Å. The geometry around the metal atom as a distorted trigonal-bipyramid is inferred from the angles

(23) Sheldrick, G. M. SHELX-76, Computer Program for crystal structure from diffraction data. University of Gottingen, Gottingen, FRG.
(24) Cromer, D. T.; Mam, J. B. *Acta. Crystallogr., Sect. A* **1968**, *A24*, 321.
(25) Cromer, D. T.; Libermann, D. J. *Chem. Phys.* **1970**, *53*, 1891.
(26) Stewart, R. F.; Davidson, E. R.; Simpson, W. T. *J. Chem. Phys.* **1965**, *42*, 3175.

**Table II.** Fractional Atomic Coordinates (×10⁴) for Non-Hydrogen Atoms (Estimated Standard Deviations in Parentheses)

| atom | x/a | y/b | z/c |
|---|---|---|---|
| Zn(1) | 6533 (1) | 8529 (1) | 3487 (1) |
| S(1) | 6759 (2) | 8431 (2) | 5387 (2) |
| S(2) | 8166 (2) | 9594 (2) | 4485 (2) |
| C(1) | 7804 (4) | 9298 (3) | 5633 (3) |
| N(1) | 8383 (4) | 9662 (2) | 6668 (2) |
| C(2) | 8000 (5) | 9549 (3) | 7665 (3) |
| C(3) | 8502 (4) | 8762 (3) | 8507 (2) |
| C(4) | 8577 (5) | 8841 (3) | 9736 (3) |
| C(5) | 9356 (4) | 10327 (3) | 6875 (4) |
| C(6) | 9116 (4) | 11363 (3) | 6697 (4) |
| C(7) | 9781 (5) | 12091 (3) | 7644 (4) |
| S(3) | 5075 (1) | 6902 (1) | 2744 (1) |
| S(4) | 7113 (1) | 7586 (1) | 2305 (1) |
| C(8) | 5941 (4) | 6832 (2) | 1935 (4) |
| N(2) | 5663 (3) | 6252 (2) | 1061 (3) |
| C(9) | 6275 (3) | 6200 (2) | 0225 (3) |
| C(10) | 7484 (2) | 5718 (2) | 0537 (3) |
| C(11) | 8207 (3) | 5843 (3) | −0260 (2) |
| C(12) | 4686 (4) | 5569 (3) | 0799 (4) |
| C(13) | 4838 (3) | 4634 (3) | 1410 (4) |
| C(14) | 3866 (4) | 3861 (3) | 0909 (3) |
| Zn(2) | 3474 (1) | 7776 (1) | 1526 (1) |
| S(5) | 3296 (1) | 7825 (1) | −0389 (1) |
| S(6) | 1840 (1) | 6721 (1) | 0528 (1) |
| C(15) | 2198 (3) | 7038 (2) | −0595 (3) |
| N(3) | 1672 (3) | 6672 (2) | −1633 (2) |
| C(16) | 1933 (4) | 6983 (3) | −2652 (3) |
| C(17) | 1419 (4) | 7913 (4) | −3209 (4) |
| C(18) | 0122 (5) | 7968 (3) | −4016 (4) |
| C(19) | 0852 (3) | 5880 (3) | −1795 (2) |
| C(20) | 1352 (4) | 4915 (3) | −1683 (3) |
| C(21) | 0508 (3) | 4099 (3) | −1947 (3) |
| S(7) | 2813 (1) | 8751 (1) | 2616 (1) |
| S(8) | 4977 (1) | 9443 (1) | 2236 (1) |
| C(22) | 3999 (3) | 9523 (2) | 2949 (3) |
| N(4) | 4065 (3) | 10217 (2) | 3656 (3) |
| C(23) | 5174 (5) | 10761 (3) | 4138 (4) |
| C(24) | 5225 (5) | 11766 (3) | 3803 (6) |
| C(25) | 6156 (4) | 12444 (3) | 4629 (4) |
| C(26) | 3039 (4) | 10505 (2) | 3937 (3) |
| C(27) | 2760 (4) | 10048 (3) | 4931 (3) |
| C(28) | 1962 (4) | 10573 (3) | 5464 (3) |

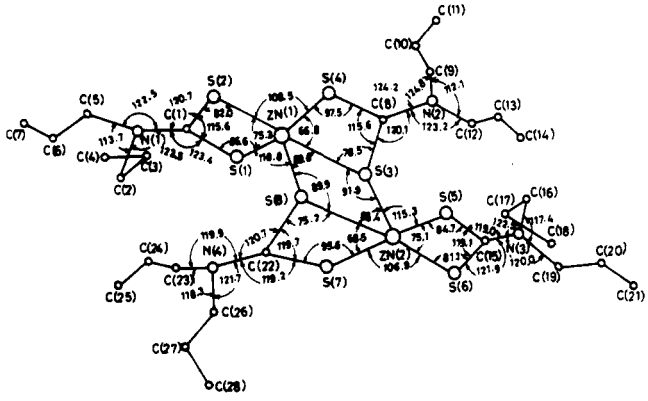

**Figure 4.** Bond angles (deg) in the $[Zn(dnpdtc)_2]_2$ molecule.

S(3)–Zn(1)–S(4) (66.8°), S(2)–Zn(1)–S(4) (108.5°), and S(3)–Zn(1)–S(2) (163.6°). Important bond lengths and bond angles are listed in Table III. For the sake of clarity, these bond lengths and bond angles are shown in Figures 3 and 4, respectively. The environment around Zn(2) is similar to that around Zn(1).

The structure is stabilized by interdimer van der Waals contacts. These van der Waals contacts are listed in a table that is included in the supplementary material.

The structure of the present compound, dimeric bis(*N*,*N*-di-*n*-propyldithiocarbamato)zinc(II), is roughly isostructural with the ethyl[18] and isopropyl[20] analogues. As in the other two structures, one of the crystallographically independent dithiocarbamato ions acts as a bridging group, linking two zinc atoms

**Table III.** Important Bond Lengths (Å) and Bond Angles (deg) in $[Zn(dnpdtc)_2]_2$ (Esd's in Parentheses)

| | | | |
|---|---|---|---|
| **Bond Lengths** | | | |
| Zn(1)–S(1) | 2.294 (3) | Zn(2)–S(5) | 2.325 (2) |
| Zn(1)–S(2) | 2.462 (3) | Zn(2)–S(6) | 2.454 (2) |
| Zn(1)–S(3) | 2.890 (2) | Zn(2)–S(7) | 2.303 (2) |
| Zn(1)–S(4) | 2.305 (2) | Zn(2)–S(8) | 2.962 (2) |
| Zn(1)–S(8) | 2.369 (1) | Zn(2)–S(3) | 2.353 (2) |
| S(1)–C(1) | 1.732 (5) | S(5)–C(15) | 1.702 (4) |
| S(2)–C(1) | 1.704 (5) | S(6)–C(15) | 1.680 (4) |
| C(1)–N(1) | 1.335 (4) | C(15)–N(13) | 1.329 (4) |
| N(1)–C(2) | 1.491 (7) | N(3)–C(16) | 1.491 (6) |
| Zn(1)–Zn(2) | 3.786 | | |
| **Bond Angles** | | | |
| S(1)–Zn(1)–S(2) | 75.3 (1) | S(5)–Zn(2)–S(6) | 75.1 (1) |
| S(2)–Zn(1)–S(4) | 108.5 (1) | S(5)–Zn(2)–S(3) | 115.2 (1) |
| S(3)–Zn(1)–S(4) | 66.8 (1) | S(3)–Zn(2)–S(8) | 88.4 (1) |
| S(1)–Zn(1)–S(8) | 118.8 (1) | S(7)–Zn(2)–S(8) | 68.5 (1) |
| S(3)–Zn(1)–S(8) | 89.8 (1) | S(7)–Zn(2)–S(6) | 106.9 (1) |
| Zn(1)–S(1)–C(1) | 86.6 (2) | Zn(2)–S(5)–C(15) | 84.7 (2) |
| Zn(1)–S(2)–C(1) | 82.0 (2) | Zn(2)–S(6)–C(15) | 81.1 (2) |
| S(1)–C(1)–S(2) | 115.6 (3) | S(5)–C(15)–S(16) | 119.1 (2) |
| S(1)–C(1)–N(1) | 123.4 (3) | S(5)–C(15)–N(3) | 119.0 (2) |
| S(2)–C(1)–N(1) | 120.7 (3) | S(6)–C(15)–N(3) | 121.9 (2) |
| Zn(1)–S(3)–Zn(2) | 91.9 (1) | Zn(1)–S(8)–Zn(2) | 89.9 (1) |

**Table IV.** Comparison of (Dialkyldithiocarbamato)zinc(II) Structures

| | $[Zn(dedtc)_2]_2$[a] | $[Zn(dipdtc)_2]_2$[b] | $[Zn(dnpdtc)_2]_2$[c] |
|---|---|---|---|
| | Distances (Å) | | |
| Zn(1)–S(1) | 2.331 | 2.335 | 2.29 |
| Zn(1)–S(2) | 2.443 | 2.454 | 2.46 |
| Zn(1)–S(3) | 2.815 | 2.815 | 2.89 |
| Zn(1)–S(4) | 2.335 | 2.342 | 2.31 |
| Zn(1)–S(8) | 2.383 | 2.377 | 2.37 |
| Zn(1)–Zn(2) | 3.546 | 3.545 | 3.78 |
| | Angles (deg) | | |
| Zn(1)–S(8)–Zn(2) | 85.37 | 85.70 | 89.9 |

[a] Reference 17. [b] Reference 19. [c] This work.

to form a dimer. A comparison of the important structural parameters of the diethyl, di-isopropyl, and di-*n*-propyl derivatives of the Zn complex is presented in Table IV. It is clear from this table that the distance between the metal ion and the bridging sulfur in $[Zn(dnpdtc)_2]_2$ (2.89 Å) is longer compared to the same distance in $[Zn(dedtc)_2]_2$ (2.815 Å) and $[Zn(dipdtc)_2]_2$ (2.815 Å), indicating a weaker intermolecular bonding in the case of the *n*-propyl derivative. Similarly, the Zn–Zn distance in the *n*-propyl derivative (3.786 Å) is substantially longer than the corresponding distance in the ethyl (3.546 Å) and in isopropyl (3.545 Å) analogues. These observations clearly reveal that dimeric bis[*N*,*N*-di-*n*-propyldithiocarbamato)zinc(II) is a weaker molecular dimer than the diethyl and di-isopropyl compounds.

**Single-Crystal EPR Studies.** Nearly 1–2% of $Cu^{2+}$ doped in dimeric bis[*N*,*N*-di-*n*-propyldithiocarbamato]zinc(II) showed no spectra associated with $Cu^{2+}$–$Cu^{2+}$ pairs. When the concentration of the dopant was increased to 4–5%, additional weaker signals were observed on either side of the strong signals due to the doublet states. The spectra were recorded in three mutually perpendicular planes, namely *ab*, *bc**, and *ac**. A sample EPR spectrum in *bc** plane when the magnetic field makes an angle of 45° with the *b* axis is shown in Figure 5. The central signals in this figure are due to the presence of a single $Cu^{2+}$—apparently with no delocalization of the spin on $Zn^{2+}$ in the $Zn^{2+}$–$Zn^{2+}$ diamagnetic system leading to a spin doublet whereas the weak signals (on both sides of the doublet signals) are due to $\Delta M_s = \pm 1$ transitions of $Cu^{2+}$–$Cu^{2+}$ pairs (triplets). Isotopic splitting due to $^{63}Cu$ and $^{65}Cu$ are evident in the doublet-state spectra whereas no such splitting is observed in the triplet-state spectra. Moreover, all the signals due to $Cu^{2+}$–$Cu^{2+}$ pairs are not seen in all the orientations because of overlap of these signals with those due to $Cu^{2+}$–$Zn^{2+}$.

The **g**- and **A**-tensor directions of the pair spectra are found to coincide whereas the **D**-tensor directions orient differently. The

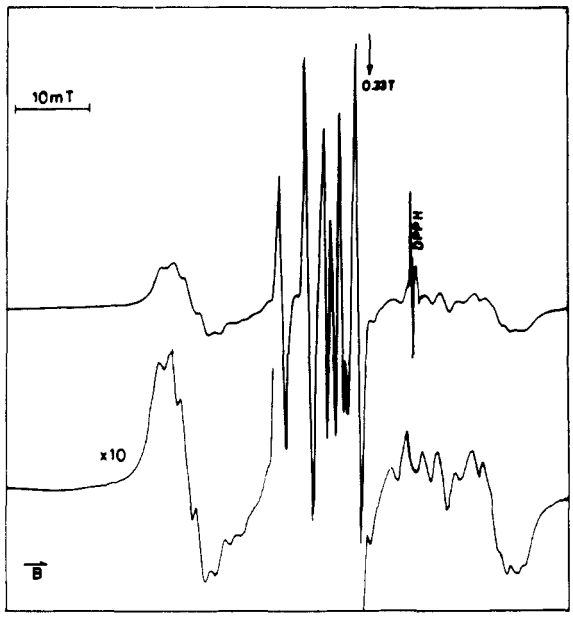


**Figure 5.** Single-crystal EPR spectra of $Cu^{2+}/[Zn(dnpdtc)_2]_2$ in the $bc^*$ plane when $B$ makes an angle of 45° with the $b$ axis.

$y$ component of the **D** tensor coincides with the $y$ direction of the **g** and **A** tensors, similar to the case of the $[Zn(dipdtc)_2]_2$ lattice.[14] But it was found that the $z$ component of the **D** tensor makes an angle of 38° ± 2° with the $g_z$ and $A_1$ directions as against 42° in the $[Zn(dipdtc)_2]_2$ lattice. Hence, the noncoinciding tensorial properties should be taken into consideration while the spin Hamiltonian parameters are derived.

**Spin Hamiltonian.** Taking cognizance of the noncoincidence of the **g** and **D** tensors in the $xz$ plane and using perturbation theory, we have derived the spin Hamiltonian for a triplet state of a coupled pair of ions with $S = {}^1/_2$. Its final form[14] is as follows:

$$\mathcal{H} = B[g_\parallel B_z S_z + g_\perp (B_x S_x + B_y S_y)] - {}^1/_3 DS(S+1) + D(\cos^2\alpha + E\sin^2\alpha)S_z^2 + (D\sin^2\alpha + E\cos^2\alpha)S_x^2 - ES_y^2 - (D-E)\sin\alpha\cos\alpha\,(S_xS_z + S_zS_x) \quad (1)$$

where "$\alpha$" is the angle between the $g_z$ and $D_1$ directions. The parameters "$D$" and "$E$" are called zero-field-splitting (ZFS) parameters. Also $D = {}^3/_2 D_1$ and $E = (D_3 - D_2)/2$ where $D_1$, $D_2$, and $D_3$ have the conventional meanings. The two fine-structure EPR transitions, corresponding to $\Delta M_s = \pm 1$, occur according to the relation

$$B_2 - B_1 \cong \frac{1}{g\beta}\left[(D\cos^2\alpha + E\sin^2\alpha)\frac{g_\perp^2}{g^2}\sin^2\theta + (D\sin^2\alpha + E\cos^2\alpha)\frac{g_\parallel^2}{g^2}\cos^2\theta + 3(D-E)\sin\alpha\cos\alpha\,\frac{g_\parallel g_\perp}{g^2}\sin\theta\cos\theta + E\right] \quad (2)$$

where "$\theta$" is the angle between the magnetic field $B$ and $g_\parallel$ directions and $g^2 = g_\parallel^2\cos^2\theta + g_\perp^2\sin^2\theta$.

Approximate spin Hamiltonian parameters and direction cosines were obtained by a least-squares fit of eq 2 in the $ac^*$ plane. Further refinement of the resonant field positions in the $ac^*$ and $bc^*$ planes was done by using a computer program, MAGNSPEC, of Kopp et al.[27] A slight rhombic component in the **g** tensor has been introduced to obtain a best fit between the experimental and calculated field positions. The hyperfine tensor was also introduced in the final calculation. The spin Hamiltonian parameters and their direction cosines obtained from the best fit of experimental and calculated field positions are listed in Table V.

**Table V.** EPR Parameters and Direction Cosines[a] of $Cu^{2+}/[Zn^{2+}(dnpdtc)_2]_2$

| param | value | direction cosines | | |
|---|---|---|---|---|
| $g_{xx}$ | 2.0182 | 0.5927 | 0.5709 | 0.5682 |
| $g_{yy}$ | 2.0126 | −0.2701 | 0.8054 | −0.5276 |
| $g_{zz}$ | 2.0726 | −0.7588 | 0.1592 | 0.6315 |
| $D_1$ | 0.018 82 cm$^{-1}$ | 0.5011 | 0.3059 | 0.8095 |
| $D_2$ | −0.006 85 cm$^{-1}$ | 0.7487 | 0.3158 | −0.5828 |
| $D_3$ | −0.011 97 cm$^{-1}$ | −0.2701 | 0.8054 | −0.5276 |
| $A_{xx}$ | 0.002 636 cm$^{-1}$ | 0.5927 | 0.5709 | 0.5682 |
| $A_{yy}$ | 0.003 192 cm$^{-1}$ | −0.2701 | 0.8054 | −0.5276 |
| $A_{zz}$ | 0.005 99 cm$^{-1}$ | −0.7588 | 0.1592 | 0.6315 |

[a] With respect to the $abc^*$ axes system.

Single-crystal EPR studies of $Cu^{2+}$–$Cu^{2+}$ pairs in bis(diethyldithiocarbamato)zinc(II) were reported by Cowsik and Srinivasan.[9] Subsequently, single-crystal EPR studies of $Ag^{2+}$–$Ag^{2+}$ pairs in bis(diisopropyldithiocarbamato)zinc(II) were reported by van Rens, van der Drift, and de Boer.[28] In a later publication, a comparison of spin Hamiltonian parameters between $Cu^{2+}$–$Cu^{2+}$ pairs and $Ag^{2+}$–$Ag^{2+}$ pairs was reported.[29] It was noticed in previous articles that, for copper as well as silver compounds, the $g$ values for the triplet species are almost equal to those of the doublet species; whereas the metal $A$ values of the triplet species are about half those of the doublet species. We have also made similar observations in our studies. Thus, it can be concluded that the electronic structure of an $M(dtc)_2$–$M(dtc)_2$ dimer (M = Cu, Ag) differs only slightly from that of an $M(dtc)_2$–$Zn(dtc)_2$ pair. These differences could be attributed to the increased spin–orbit coupling values for the $Ag^{2+}$ ion as well as the increased radial expansion of the 4d orbitals and the consequent increase in covalency.

**Low-Temperature EPR Studies on Polycrystalline Samples.** It was evident from the room-temperature EPR studies of $Cu^{2+}$ in bis(*N*,*N*-di-*n*-propyldithiocarbamato)zinc(II) that considerable spin–spin interaction between the two adjacent metal centers exists. In order to get an idea of the nature of magnetic isotropic exchange interactions for $Cu^{2+}$–$Cu^{2+}$ pairs in the host lattice, we have carried out variable-temperature EPR studies on powder samples.

During our low-temperature studies two important observations were made. They are (i) the magnitude of the zero-field-splitting parameter ($D$) increases as the temperature is lowered and (ii) the intensity of all the signals (due to $\Delta M_s = \pm 1$ as well as $\Delta M_s = \pm 2$ transitions of the triplet states) increases considerably with the lowering of temperature.

**Temperature Dependence of ZFS Parameter.** It was observed during low-temperature EPR studies on polycrystalline samples that the signals due to $\Delta M_s = \pm 1$ transitions of $Cu^{2+}$–$Cu^{2+}$ pairs move outward, both in low-field and high-field regions, as the temperature is lowered. But, the positions of the signals due to doublet states remained static. Since the separation between the centers of two fine-structure transitions in the parallel region correspond to twice the value of $D$, the above observation clearly suggests that the magnitude of $D$ increases as the temperature is lowered. The increase of $D$ at low temperatures is quite significant. Figure 6 shows the polycrystalline EPR spectra of $Cu^{2+}/Zn^{2+}(dnpdtc)_2$ at two temperatures, $T$ = 297 and 20 K. The variation of the experimental $D$ values with temperature is shown in Figure 7.

The above observation of increase in $D$ with lowering of temperature can be explained in terms of a possible crystal contraction of the host lattice at low temperatures. The possibility of a phase transition can be ruled out, since there are no drastic changes in the pattern of the EPR signal. However, the exact proof for a

(27) (a) Mackey, J. H.; Kopp, M.; Tynan, E. C.; Fu Yen, T. In *Electron Spin Resonance in Metal Complexes*; Fu Yen, T., Ed.; Plenum Press: New York, 1969; p 33. (b) Kopp, M.; Mackey, J. H. *J. Comput. Phys.* **1969**, *3*, 539.

(28) van Rens, J. G. M.; van der Drift, E.; de Boer, E. *Chem. Phys. Lett.* **1972**, *14*, 113.

(29) van Rens, J. G. M.; de Boer, E. *Chem. Phys. Lett.* **1975**, *31*, 377.

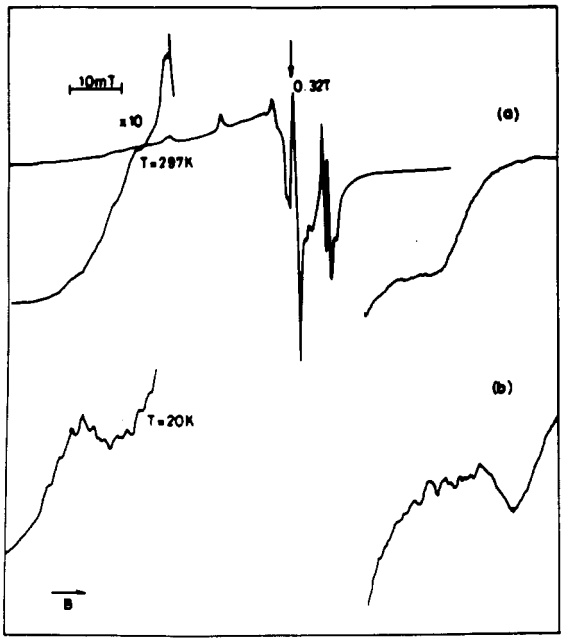


**Figure 6.** Polycrystalline EPR spectra of $Cu^{2+}/[Zn(dnpdtc)_2]_2$: (a) at $T$ = 300 K; (b) at $T$ = 20 K.

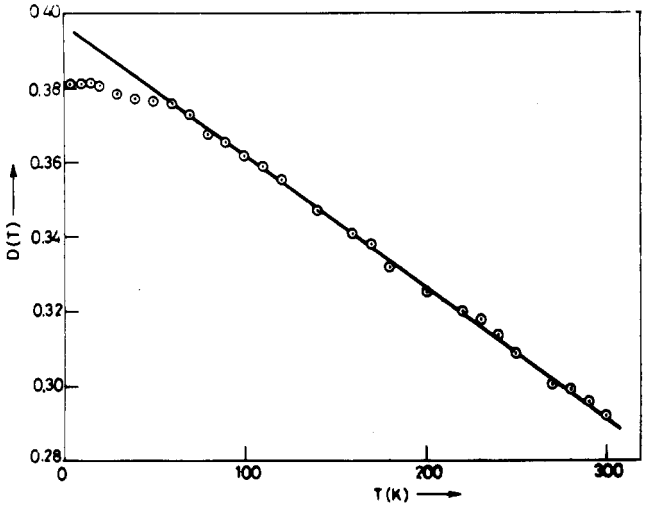


**Figure 7.** Variation of zero-field-splitting parameter ($D$) with temperature in the $Cu^{2+}/[Zn(dnpdtc)_2]_2$ system.

possible crystal contraction should come from a complete X-ray crystal structure of the host lattice at low temperatures.

**Half-Field ($\Delta M_s = \pm 2$) Transition.** It is known that when the magnitude of the ZFS parameter ($D$) is sufficiently large, one would expect the occurrence of $\Delta M_s = \pm 2$ transitions within the triplet manifold. In our studies of $Cu^{2+}$–$Cu^{2+}$ pairs in the $[Zn(dnpdtc)_2]_2$ lattice, we have observed this transition at room temperature itself. This signal is centered around 0.163 T with a few of the hyperfine lines resolved.

It was found during our low-temperature EPR studies that the intensity of this $\Delta M_s = \pm 2$ transition increases drastically as the temperature is lowered. This increase in intensity is more than that expected from the Boltzmann population difference within the triplet manifold. Half-field transitions at two temperatures shown in Figure 8 reveal the differences in the intensities. It appears that the isotropic exchange interaction between the two interacting spins of the dimeric unit is of "ferromagnetic" nature (triplet ground state). The signal intensities of these half-field

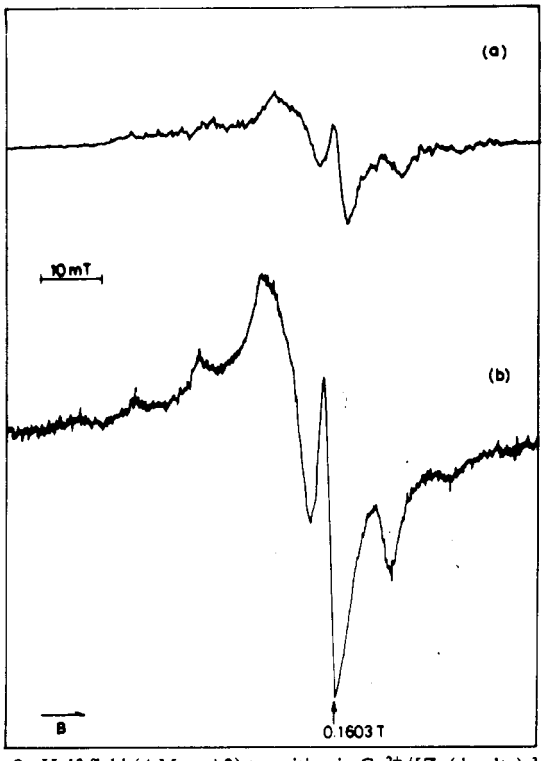


**Figure 8.** Half-field ($\Delta M_s = \pm 2$) transition in $Cu^{2+}/[Zn(dnpdtc)_2]_2$: (a) at $T$ = 300 K; (b) at $T$ = 77 K.

transitions at various temperatures have been utilized to evaluate the magnitude of the isotropic exchange coupling constant.

The magnitude of the exchange-coupling constant for $Cu^{2+}$–$Cu^{2+}$ pairs in the $[Zn(dnpdtc)_2]_2$ lattice has been obtained by the procedure described in detail in our previous publication.[14] This procedure is based on the least-squares fitting of the experimental EPR signal intensities of $\Delta M_s = \pm 2$ transitions at various temperatures with the corresponding calculated intensities. The isotropic exchange-coupling constant, $2J$, obtained for this system is +13 $cm^{-1}$, making it a ferromagnetically coupled dimer.

## Conclusions

The crystal structure solution has given proof for the existence of dimeric units in the bis[N,N-di-n-propyldithiocarbamato]-zinc(II) lattice. The triplet-state EPR studies of isolated $Cu^{2+}$–$Cu^{2+}$ pairs in this lattice have clearly revealed that the nature of isotropic exchange interaction is of ferromagnetic origin, like in other related dithiocarbamato dimeric systems. The considerable increase in the magnitude of the zero-field-splitting parameter has led us to conclude that the host lattice undergoes a slight crystal contraction at lower temperatures. The possible crystal contraction of the host lattice can only be confirmed by solving the complete X-ray crystal structure at some low temperature.

**Acknowledgment.** N.S. thanks the Indian Institute of Technology, Madras, India, for financial assistance in the form of a research fellowship. This work was also supported by a grant from the Department of Science and Technology, Government of India, New Delhi.

**Registry No.** $[Zn(dnpdtc)_2]_2$, 128973-31-9; $[Cu(dnpdtc)_2]_2$, 40437-78-3.

**Supplementary Material Available:** Tables SI–SIV, listing anisotropic thermal parameters, least-squares mean planes, interdimer distances making van der Waals contacts, and relevant torsion angles (7 pages); a table of structure factor amplitudes (12 pages). Ordering information is given on any current masthead page.